lanthanum acetate. It is clear that the paramagnetic shifts are substantial compared with the diamagnetic references, and as in solution applications of such compounds, the magnetic anisotropy may lead to significant changes in the positions compared with those expected from simple bonding pattern analogies.

Acknowledgment. This work was supported by the National Institutes of Health, GM-29428 and GM-34541. Helpful discussions with Professor Doyle Britton, University of Minnesota, are gratefully acknowledged.

Registry No. Pr(III) acetate·H_2O, 17829-83-3; Eu(III) acetate·$3H_2O$, 101953-41-7.

Supplementary Material Available: Positional and thermal parameters and their esd's (85 pages). Ordering information is given on any current masthead page.

Determining the Structure of a Glycopeptide–Ac_2-Lys-D-Ala-D-Ala Complex Using NMR Parameters and Molecular Modeling

S. W. Fesik,* T. J. O'Donnell, R. T. Gampe, Jr., and E. T. Olejniczak

Contribution from the Pharmaceutical Discovery Division, Abbott Laboratories, Abbott Park, Illinois 60064. *Received November 6, 1985*

Abstract: The interaction between ristocetin pseudo-aglycon and Ac_2-Lys-D-Ala-D-Ala, a model for the antibiotics' binding site of action, has been examined with NMR spectroscopy and molecular modeling. From a multispin analysis of the cross-peak volumes measured from a series of two-dimensional NOE experiments, many, accurate, proton–proton distances were obtained. These distance constraints along with vicinal spin–spin coupling constants and NH exchange rates were used to evaluate and modify computer-generated structures of the complex. Structures of the complex were energy minimized by applying different force fields, including one which contained an extra term, $K(r - r_0)^2$, used to constrain the interproton distances (r) in the computer-generated structure to the experimentally determined distances (r_0). Additional structures were generated from a short molecular dynamics trajectory. Two representative conformations were selected, minimized, and compared to the measured proton–proton distances. No single conformation was sufficient to explain all of the NMR data. The data were best explained by considering an average structure.

Vancomycin, a clinically useful glycopeptide antibiotic, has proven to be the drug of choice against methicillin resistant gram-positive bacteria.[1] Due to the recent increase of these types of infections,[2] vancomycin[3] and other members of this class of antibiotics (ristocetin,[4] avoparcin,[5] and teicoplanin[6]) have received a considerable amount of attention. It is believed that the glycopeptide antibiotics exert their antibiotic activity by binding to cell wall precursors terminating in D-alanyl-D-alanine.[7] In fact, the binding of di- and tripeptide models (Ac-D-Ala-D-Ala and Ac_2-Lys-D-Ala-D-Ala) of cell wall precursors correlates well with their antibiotic potencies.[8,9]

Using nuclear magnetic resonance spectroscopy, several investigators[10-13] have studied the structures of glycopeptide–peptide complexes. On the basis of the NMR data, the D-Ala-D-Ala binding site was found to be qualitatively similar in these studies; however, the proposed location of the Lys residue was found to be markedly different, depending on the antibiotic or solvent used in the study. Several other discrepancies exist in the structural models proposed for glycopeptide–peptide complexes. For example, Williams and co-workers[4,14] have postulated that an electrostatic interaction between the carboxylate anion of the peptide and the protonated amino terminus of ristocetin was important in the formation of the complex. Recently, however, the importance of this electrostatic interaction was questioned,[9] since a series of ristocetin analogues lacking a positively charged amino group all possessed antibacterial activity and were found to bind to Ac_2-Lys-D-Ala-D-Ala.

In addition to resolving the remaining ambiguities on the structure(s) of glycopeptide–peptide complexes, our studies are aimed at obtaining more detailed structures of the complexes than those previously reported. An important consideration in our work is how to use dynamic averaged NMR parameters to derive a structure or set of structures which represent the low-energy conformations about which most fluctuations occur. To obtain highly resolved structures, a large number of accurate distance constraints are required. Also, computational methods are needed to generate structures based on these distance constraints that are energetically reasonable and that can be quantitatively evaluated in terms of experimentally determined parameters.

In this report we have examined the interaction between ristocetin pseudo-aglycon and Ac_2-Lys-D-Ala-D-Ala in CD_3OD and CD_3OH. From a quantitative analysis of pure absorption two-dimensional NOE data sets, many accurate interproton distance constraints were obtained. These distance constraints along with spin–spin coupling constants and NH exchange rates were used to evaluate and modify computer graphical models of the complex generated from standard bond lengths and angles. Several ap-

(1) Griffith, R. S. *J. Antimicrob. Chemother.* **1984**, *14*, Suppl. D, 1.
(2) Crossley, K.; Loesch, D.; Landesman, B.; Mead, K.; Chern, M.; Strate, R. *J. Infect. Dis.* **1979**, *139*, 273.
(3) Farber, B. B. *Eur. J. Clin. Microbiol.* **1984**, *3*, 1.
(4) Williamson, M. P.; Williams, D. H.; Hammond, S. J. *Tetrahedron* **1984**, *40*, 569.
(5) (a) Ellestad, G. A.; Leese, R. A.; Morton, G. O.; Barbatschi, F.; Gore, W. E.; McGahren, W. J. *J. Am. Chem. Soc.* **1981**, *103*, 6522. (b) Fesik, S. W.; Armitage, I. M.; Ellestad, G. A.; McGahren, W. J. *Mol. Pharmacol.* **1984**, *25*, 275.
(6) (a) Borghi, A.; Coronelli, C.; Faniuolo, L.; Allievi, G.; Pallanza, R.; Gallo, G. G. *J. Antibiot.* **1984**, *37*, 615. (b) Hunt, A. H.; Molloy, R. M.; Occolowitz, J. L.; Marconi, G. G.; Debono, M. *J. Am. Chem. Soc.* **1984**, *106*, 4891. (c) Barna, J. C. J.; Williams, D. H.; Stone, D. J. M.; Leung, T. W. C.; Doddrell, D. M. *J. Am. Chem. Soc.* **1984**, *106*, 4895.
(7) Williams, D. H.; Rajananda, Vi.; Williamson, M. P.; Bojesen, G. In *Topics in Antibiotic Chemistry*; Sammes, P. G., Ed.; John Wiley & Sons, Inc.: New York, 1980; Vol. 5, p 119.
(8) Nieto, M.; Perkins, H. R. *Biochem. J.* **1971**, *124*, 845.
(9) Herrin, T. R.; Thomas, A. M.; Perun, T. J.; Mao, J. C.; Fesik, S. W. *J. Med. Chem.* **1985**, *28*, 1371.
(10) Convert, O.; Bongini, A.; Feeney, J. *J. Chem. Soc., Perkin Trans. 2* **1980**, 1262.
(11) Williams, D. H.; Williamson, M. P.; Butcher, D. W.; Hammond, S. J. *J. Am. Chem. Soc.* **1983**, *105*, 1332.
(12) Fesik, S. W.; Armitage, I. M.; Ellestad, G. A.; McGahren, W. J. *Mol. Pharmacol.* **1984**, *25*, 281.
(13) Williamson, M. P.; Williams, D. H. *J. Chem. Soc., Perkin Trans. 1* **1985**, 949.
(14) Barna, J. C. J.; Williams, D. H.; Williamson, M. P. *J. Chem. Soc., Chem. Commun.* **1985**, 254.

0002-7863/86/1508-3165$01.50/0

proaches were used to incorporate the NMR data in the generation of energetically feasible structures. The methodologies employed and the relevance of the structures obtained are discussed.

Experimental Section

A 1:1 mixture of ristocetin pseudo-aglycon (20 mM) and Ac_2-Lys-D-Ala-D-Ala (20 mM) was prepared in CD_3OD and CD_3OH. NMR signals were in slow exchange on the NMR time scale consistent with the association constant (6.4×10^5)[9] measured for this complex in aqueous solution. NMR spectra were recorded at 25 °C on a Nicolet NT-360 NMR spectrometer. Correlated spectroscopy (COSY)[15] experiments were acquired with use of a (D5–90°–t_1–90°–acquire)$_n$ pulse sequence and processed in the absolute value mode applying a sinebell window function in each dimension before Fourier transformation. For the pure phase 2D NOE[16] experiments, a (D5–90°–t_1–90°–τ_m–90°—acquire)$_n$ pulse sequence was employed by using a sweep width of 6666 Hz with the carrier frequency to the downfield side of the spectrum. Seven 512 × 1 K 2D NOE data sets with mixing times of 75, 150, 250, 350, 500, 750, and 1000 ms were acquired of the complex dissolved in CD_3OD by using a D5 value of 1.9 s. For the COSY and 2D NOE data sets recorded of the complex in CD_3OH, the large solvent signal was irradiated during the recycle delay, D5, before the first pulse and during τ_m. Mixing times of 75, 150, and 300 ms were used for the 2D NOE data sets acquired in CD_3OH. The pure phase 2D NOE data sets were processed with use of a modified version of FTNMR obtained from Dr. D. Hare. A complex FFT was performed in t_2 after apodization and zero filling to 2048 complex points. A real FFT was performed in t_1 after applying a cosine window function and zero filling to 1024 points. Subsequently, a base line correction was applied by using a fifth-order polynomial in ω_1. The volumes of the cross peaks and diagonal peaks were integrated from the unsymmetrized 2D data sets by choosing an integration radius and summing over all data points within the chosen radius.

Distances were calculated from the cross peak and diagonal peak volumes as previously described.[17] First, a relaxation rate matrix, Γ, was obtained[18] from the volume matrix, $V(\tau_m)$, of cross and diagonal peak volumes by using

$$V(\tau_m) = (e^{-\Gamma\tau_m})V^0 \quad (1)$$

where V^0 is the volume at $\tau_m = 0$ and Γ is a matrix of relaxation rates. The matrix has the form

$$\Gamma = \begin{bmatrix} \rho_1 & \sigma_{12} & \sigma_{13} & \cdots \\ \sigma_{21} & \rho_2 & & \\ & & \ddots & \\ & & & \rho_n \end{bmatrix} \quad (2)$$

This can be rearranged to give Γ in terms of $V(\tau_m)$ and V^0 as[17,18]

$$-\frac{\ln (V(\tau_m)(V^0)^{-1})}{\tau_m} = \Gamma \quad (3)$$

This equation is easily solved by rewriting it in terms of the matrix of eigenvectors, [X], and the diagonal matrix of eigenvalues, [D], of $V(\tau_m)(V^0)^{-1}$.[17,18]

$$-\frac{[X] \ln [D][X]^{-1}}{\tau_m} = \Gamma \quad (4)$$

From the cross-relaxation rates, σ, and a known distance, r_{kl}, unknown distances, r_{ij}, can be calculated by assuming that the dynamics of both internuclear vectors are the same[19] using the equation

$$r_{ij} = \left[r_k^6 \quad \frac{\sigma_{kl}}{\sigma_{ij}} \right]^{1/6} \quad (5)$$

Our known distance was chosen to be the distance between the ortho protons of the A, C, and G rings which is 2.48 Å based on calculations

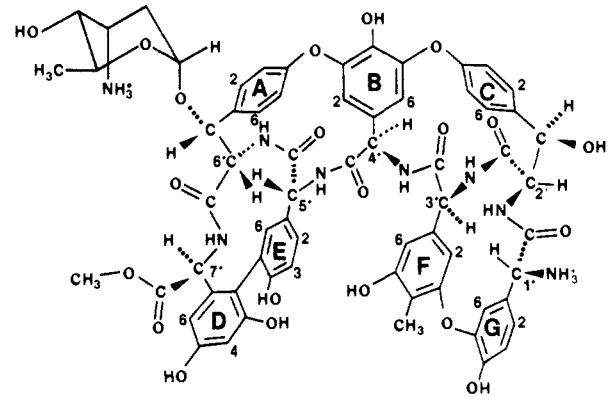

Figure 1. The structure of ristocetin pseudo-aglycon.

using standard bond lengths and bond angles.[20] The distances calculated from the relaxation rates measured for these three sets of ortho protons were nearly identical (+/–0.1 Å), suggesting that for at least these portions of the molecule the assumption of identical dynamics used in eq 5 is valid.

Computer models of ristocetin aglycone and Ac_2-Lys-D-Ala-D-Ala were generated from standard bond angles and bond lengths supplied to the AMBER[21] modeling program. With use of the Abbott Computerized Molecular Design System,[22] the torsional angles of ristocetin aglycon were adjusted to accommodate the four additional cross-linking bonds between the A–B, B–C, D–E, and F–G rings (see Figure 1). The initial tripeptide structure was based on the reported crystal structure of Ac-Ala-Ala.[23] The tripeptide and the ristocetin aglycone structures were independently optimized using AMBER energy minimization.

A computer model of the ristocetin aglycone–tripeptide complex was made by interactively docking the two molecules on a computer graphics terminal. The relative positions of the two molecules were chosen to qualitatively agree with the NMR data. The complex was optimized with use of AMBER energy minimization and resulted in a structure having an energy lower than the sum of the AMBER energies of the two isolated components, as expected for a bound complex. Details of this computation will be published elsewhere. Since our version of AMBER only implicitly included the protons as part of the atom to which they are attached (united atom approach), the valence force field (VFF) of Hagler and co-workers,[24] which treated the protons explicitly in the computer modeling, was used. To include the distance constraints obtained from the NOE data, another term was added to the force field of the form

$$E = \ldots + K(r - r_0)^2 \quad (6)$$

where r_0 is the experimentally determined proton–proton distance, r is the computed distance, and K is a pseudobond force constant. With use of this modified force field, several VFF energy minimizations were performed, starting with the previously optimized AMBER structure of the complex. Using values ranging from 10 to 100 kcal/mol/Å^2 for K resulted in the same optimized structure.

In addition to energy minimization, the VFF program[24] was used for molecular dynamics calculations. Starting with the minimized structure of the complex from the AMBER force field, 100 structures of the complex were selected at 0.1-ps intervals from a 10-ps-dynamics trajectory run at 300 K. Average interproton distances, r_{av}, were calculated from the structures generated in the dynamics trajectory without further energy minimization from

$$r_{av} = \left[\frac{4\pi}{5} \sum_{n=-2}^{2} \left| \frac{\langle Y_n^2(\phi,\theta) \rangle}{r^3} \right|^2 \right]^{-1/6} \quad (7)$$

where r = interproton distance (Å), Y_n^2 = second-order spherical harmonic, and ϕ and θ are polar angles. This is close to a simple $1/r^6$ average for the 100 dynamics conformations which also takes into account any angular averaging which would affect the measured relaxation

(15) Aue, W. P.; Bartholdi, E.; Ernst, R. R. *J. Chem. Phys.* **1976**, *64*, 2229.
(16) Bodenhausen, G.; Kogler, H.; Ernst, R. R. *J. Magn. Reson.* **1984**, *58*, 370.
(17) Olejniczak, E. T.; Gampe, R. T.; Fesik, S. W. *J. Magn. Reson.* **1986**, *67*, 28.
(18) (a) Bremer, J.; Mendz, G. L.; Moore, W. J. *J. Am. Chem. Soc.* **1984**, *106*, 4691. (b) Perrin, C. L.; Gipe, R. K. *J. Am. Chem. Soc.* **1984**, *106*, 4036.
(19) Noggle, J. H.; Shirmer, R. E. *The Nuclear Overhauser Effect. Chemical Applications*; Academic Press: New York, 1971.
(20) Pople, J. A.; Beveridge, D. L. *Approximate Molecular Orbital Theory*; McGraw Hill: New York, 1970; p 111.
(21) Weiner, S.; Kollman, P. A.; Case, D.; Singh, U. C.; Ghio, C.; Algona, G.; Weiner, P. *J. Am. Chem. Soc.* **1984**, *106*, 765.
(22) Martin, Y. C.; Kim, K. H.; Koschmann, T.; O'Donnell, T. J. In *Computer Applications in Chemistry*; Heller, S. R., Potenzone, R., Jr., Eds.; Elsevier Science Publishers B.V.; Amsterdam, 1983; pp 285–301.
(23) Fletterick, R. J.; Tsai, C.; Hughes, R. E. *J. Phys. Chem.* **1971**, *75*, 118.
(24) Lifson, S.; Hagler, A. T.; Dauber, P. *J. Am. Chem. Soc.* **1979**, *101*, 5111.

Table I. Proton Chemical Shift Assignments of 20 mM Ristocetin Pseudo-Aglycon-Ac_2-Lys-D-Ala-D-Ala (1:1) in Methanol[a]

proton	δ	proton	δ	proton	δ	proton	δ
NH2	11.53	C3	6.92	3′	5.47	R-4	3.61
NH7	9.52	E2	6.87	C_{Bz}	5.37	R-5	3.61
NH3	9.50	G6	6.83	A_{Bz}	5.20	Lys-ϵCH_2	3.23
NH4	9.16	NH6	6.83	1′	5.16	R-2a	2.45
LysNH(α)	8.29	E3	6.82	R-1	5.07	R-2b	2.23
^{1}AlaNH	8.13	G3	6.75	B2	5.03	Lys-$COCH_3(\alpha)$	2.10
LysNH(ϵ)	8.04	F2	6.73	5′	4.85	F-CH_3	2.06
E6	7.87	A5	6.59	6′	4.68	Lys-$COCH_3(\epsilon)$	1.98
C6	7.86	F6	6.47	7′	4.67	R-6	1.46
^{2}AlaNH	7.85	D4	6.45	^{2}AlaαCH	4.60	$^2AlaCH_3$	1.19
C2	7.11	4′	6.24	LysαCH	4.23	$^1AlaCH_3$	0.58
A6	7.08	D6	6.22	R-3	4.23		
C5	7.06	B6	5.67	^{1}AlaαCH	4.07		
G2	7.01	2′	5.49	$COOCH_3$	3.86		

[a] R designates a ristosamine proton.

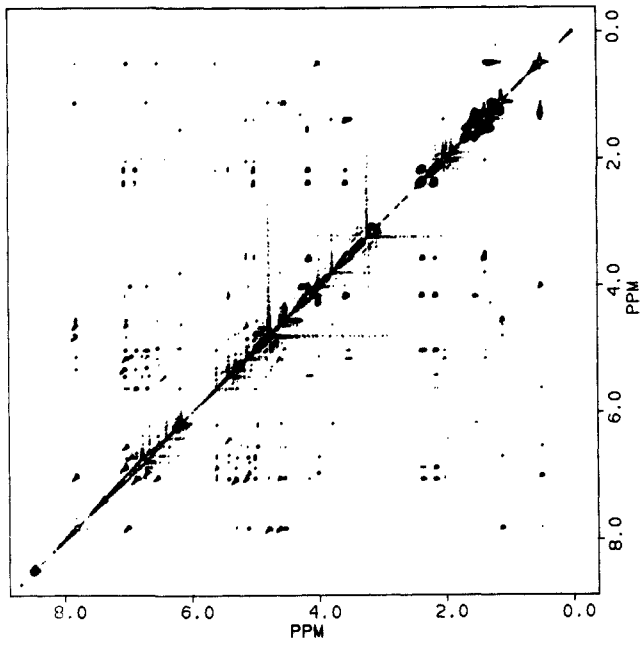

Figure 2. Pure absorption 2D NOE contour map of ristocetin pseudo-aglycon-Ac_2-Lys-D-Ala-D-Ala (1:1) complex in CD_3OD. Data were acquired with use of a mixing time of 250 ms.

rates.[25] Average dihedral angles were obtained from the average coupling constants extracted for each of the structures generated in the dynamics run.

Results

The proton NMR resonances of the ristocetin pseudo-aglycon-Ac_2-Lys-D-Ala-D-Ala complex were assigned by identifying the scalar coupled protons from correlated spectroscopy (COSY) and the dipolar coupled protons through two-dimensional nuclear Overhauser effect (2D NOE) experiments. Table I lists the proton assignments of the complex with the numbering scheme shown in Figure 1.

In order to obtain a detailed structure of the antibiotic-tripeptide complex, we obtained many, accurate interproton distances from NOE experiments. Since one-dimensional NOE experiments are limited due to nonselectivity of the preirradiation, two-dimensional NOE methods were employed. Figure 2 depicts a contour map of a 2D NOE experiment of the ristocetin pseudo-aglycon-Ac_2-Lys-D-Ala-D-Ala complex in CD_3OD acquired with a mixing time of 250 ms. Several cross peaks (~100) can be observed in the contour map corresponding to short proton-proton distances. For an accurate determination of distances from the 2D NOE data, spin diffusion and other multispin effects must be taken into account.[26] Therefore, a multispin analysis of the

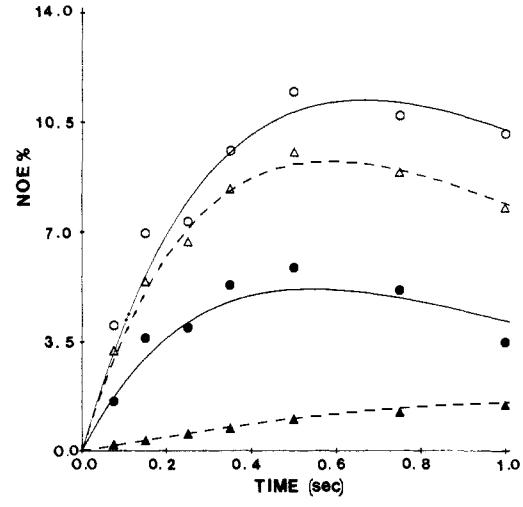

Figure 3. Experimental 2D NOE data (O = A6-A5; Δ = A6-A_{BZ}; ● = ^{2}AlaαCH-$^2AlaCH_3$; ▲ = A5-6′) compared to multispin simulations based on the measured relaxation matrix. The "NOE %" is defined as the ratio of the cross-peak volume to the equilibrium single proton volume.

cross-peak volumes obtained from seven 2D NOE data sets acquired with mixing times of 75, 150, 250, 350, 500, 750, and 1000 ms was performed. Figure 3 depicts representative examples of our NOE data, including simulations based on the measured relaxation matrix. By taking into account multispin effects, the time development curves could be analyzed in considerable detail. As described elsewhere,[17] subtle features of the curves, such as the lag or induction periods, could be accounted for, resulting in a more accurate analysis of the data. Even though multispin effects were taken into consideration in our analysis, errors, predominantly those occurring from inaccurate cross-peak volume measurements, contribute to our reported distances. If we assume that the resulting errors in the measured relaxation constants are independent of the size of the relaxation constant, then the uncertainty in our distance calibration should go as

$$\Delta r = K\frac{\Delta\sigma}{\sigma^{7/6}} \tag{8}$$

$\Delta\sigma$ can be estimated from the differences in the relaxation constants determined from the seven different mixing times. From this analysis we estimate our errors in distance measurements to be ±0.1, 0.3, and 0.7 Å for distance measurements at 2.5, 3.0, and 3.5 Å, respectively. A list of some of the proton-proton distances calculated from the 2D NOE data is given in Table II.

NOEs involving the NH protons of the complex also provided useful structural information. The NH protons were assigned from COSY and 2D NOE experiments of the complex in CD_3OH in which the large solvent peak was suppressed by preirradiation.

(25) Olejniczak, E. T.; Dobson, C. M.; Karplus, M.; Levy, R. M. *J. Am. Chem. Soc.* **1984**, *106*, 1923.

(26) Keepers, J. W.; James, T. L. *J. Magn. Reson.* **1984**, *57*, 404.

Table II. Proton–Proton Distances Obtained Experimentally from 2D NOE Data Analysis Compared to Distances Measured from Computer-Generated Structures[a]

		interproton distance (Å)		
proton–proton	from NOE	structure I	structure II	dynamics av
^{1}AlaαCH-1′	4.7	4.26	4.14	4.09
^{1}AlaαCH-G2	3.1	2.98	3.28	3.33
^{1}AlaαCH-G3	3.6	2.58	2.90	3.29
^{1}AlaCH$_3$-C5	3.0	3.33	3.60	3.43
^{2}AlaαCH-A6	2.9	3.10	3.28	3.30
^{2}AlaCH$_3$-E$_6$	3.4	3.48	3.95	3.59
^{2}AlaCH$_3$-G3	3.5	5.25	5.56	4.70
LysCH$_3$(α)-A$_{BZ}$	3.8	3.06	2.94	3.40
LysCH$_3$(α)-A6	4.7	4.71	4.57	4.70
A5-B2	3.3	3.13	3.02	3.12
A5-6′	4.2	4.50	4.45	4.57
A6-A$_{BZ}$	2.5	2.45	2.46	2.51
A6-6′	2.9	2.85	2.78	2.84
A$_{BZ}$-6′	2.7	2.47	2.47	2.46
C6-1′	3.4	3.54	3.65	3.78
E6-5′	2.4	2.25	2.25	2.26
E6-6′	2.5	2.88	2.92	2.73
F2-G6	2.7	2.42	2.94	2.78
F2-3′	3.5	3.37	3.83	3.82
F6-3′	2.7	2.96	2.34	2.67
G2-1′	2.5	2.41	2.50	2.56
G6-1′	3.5	3.78	3.71	3.76
NH2–NH3	2.6	2.38	2.42	2.41
NH3–NH4	2.5	2.28	2.25	2.31
NH3–F2	2.4	2.72	2.60	2.79
NH4–B6	3.1	3.19	3.15	3.10
NH4–F2	2.9	3.89	2.55	2.79

[a] Effective distances to the methyl groups were calculated from the approximation[30] $r = (1/3\sum_{i=1}^{3} 1/r^6)^{-1/6}$.

Two-dimensional NOE data sets were acquired with mixing times of 75, 150, and 300 ms. Proton–proton distances calculated from the NOE data appear in Table II.

In addition to the NOE data, vicinal spin–spin coupling constants were obtained and analyzed in terms of dihedral angles (Table III), and NH exchange rates of the amide protons were measured (Table IV).

Discussion

Several intermolecular NOEs are particularly important in defining the structure of the complex. NOEs between the ^{1}AlaCH$_3$ protons and the A5, C5, and B6 protons of the antibiotic suggest that the methyl group is located over the B ring and is consistent with the upfield shift (0.5 ppm) observed for the ^{1}AlaCH$_3$ protons. NOEs between the ^{1}AlaαCH proton and the G2, G3, and 1′ proton of ristocetin pseudo-aglycone indicate that the G ring is also in close proximity (on the opposite side) to the ^{1}Ala residue. The binding site of the middle ^{2}Ala residue of the tripeptide is defined by several NOEs including ^{2}AlaCH$_3$ to G3 and E6 and ^{2}AlaαCH to A6, A5, and E6. The location of the Lys residue is defined by NOEs observed between the Lys CH$_3$(α) protons and the A$_{BZ}$, A6, and anomeric and CH$_3$ protons of the sugar. These results are consistent with the αCH proton of the lysine residue pointing away from the antibiotic and the lysine side chain oriented over the D ring of the glycopeptide. Indeed, a weak NOE was observed between the Lys β-CH$_2$ protons and the D6 proton of the antibiotic.

In addition to the use of intermolecular NOEs to define the structure of the complex, intramolecular NOEs were used to determine the bound conformations of the individual components of the complex. NOEs observed between ^{1}AlaNH and ^{2}AlaαCH and between ^{2}AlaNH and LysαCH suggest that the tripeptide is in an extended conformation. For ristocetin pseudo-aglycon, NOEs between the E6 and 5′, 6′, and A$_{BZ}$ protons define the shape of this part of the molecule. The conformation of the other half of the antibiotic is defined by NOEs between C6-1′, G2-1′, F2-3′, F6-3′, NH4-F2, and NH3-F2.

From standard bond lengths and bond angles, a structure of the complex was generated by using the amino acid library of the AMBER molecule mechanics program. The structure was interactively manipulated to qualitatively agree with the NOE and vicinal coupling constant data. The resulting structure served as a starting structure in subsequent energy minimizations using either AMBER or VFF. Proton–proton distances computed from the VFF energy minimized structures were compared to interproton distances calculated from our 2D NOE data sets. Although the majority of the experimentally determined distances fit the computer-generated structures (e.g., structure I in Figure 4A) as shown in Table II, a few discrepancies remained. To generate a structure which would be forced to quantitatively agree with our NOE derived distances, an extra term was added to the force field (see Experimental) and fifteen distance constraints were applied. The force constant, K, was used to adjust the energy contribution of these proton–proton pseudobonds. The structure that resulted from these calculations agreed with the experimentally determined distances included as constraints. However, subsequent relaxation of this structure, in which the pseudobond constraints were removed, again gave a structure which did not fit all of the NOE data. In fact, the new structure was almost identical with the previously minimized structure (structure I).

Since our NMR data were inconsistent with any one low-energy structure, we considered the possibility of motional averaging. To generate additional structures, a molecular dynamics run was performed on the complex in 1.0 fs time steps for a total time of 10 ps. From this short dynamics run, 100 structures separated by 0.1 ps in the dynamics run were selected. Of these structures, very small changes were observed for the tripeptide and ristocetin aglycon peptide backbone. For the most part, the hydrogen bonds holding the two peptides together remained intact throughout the dynamics run. In contrast, the location of the Lys side chain beyond the γCH$_2$ protons was quite variable, consistent with the lack of NOEs observed for the LysCH$_3$(ε) and ε-CH_2 protons in CD$_3$OD, but inconsistent with the NOEs observed[13] for the ε-CH$_2$ protons in D$_2$O. The only other portions of the complex undergoing large amplitude motions were the F and G rings. One of the substantially altered conformations that was generated in the dynamics run was used as a starting structure for energy minimization. Figure 4B depicts this new structure (structure II). As shown at the bottom of Figure 4, the major difference between these structures is in the relative orientations of the F and G rings.

Table III. Dihedral Angles Obtained Experimentally from Vicinal Spin–Spin Coupling Constants ($^3J_{NH-\alpha CH}$) Compared to Dihedral Angles Measured from Computer-Generated Structures[a]

		dihedral angles			
NH-αCH	$^3J_{NH-\alpha CH}$ (Hz)	from J values	structure I	structure II	RMS dynamics av[b]
NH2-2′	10.3	165.5	177.8	−177.8	167.0
NH3-3′	10.3	165.5	166.2	176.8	161.7
NH4-4′	9.2	155.8	140.4	144.2	145.8
NH7-7′	5.0	130.3 (40.5)	−125.8	−119.8	113.4
^{1}AlaαNH-αCH	7.5	144.2 (21.5)	−137.1	−147.3	128.3
^{2}AlaNH-αCH	5.5	133.0 (37.0)	−141.5	−138.4	130.3
LysNH-αCH	5.8	134.5 (35.0)	−140.5	−144.8	147.2

[a] Assumes the following form[31] for the Karplus equation: $^3J_{NH\alpha CH} = 9.4\cos^2\theta - 1.1\cos\theta + 0.4$. The sign of the dihedral angle cannot be determined from the measured coupling constants. [b] The average dihedral angle calculated from the coupling constants in 100 coordinated sets separated by 0.1 ps in the dynamics run.

Table IV. NH Exchange Rates (k_{ex}) for the Amide Protons in the Ristocetin Pseudo-Aglycon-Ac_2-Lys-D-Ala-D-Ala Complex

proton	k_{ex} (min^{-1})	proton	k_{ex} (min^{-1})
NH4	0.005	LysNH(α)	0.052
NH3	0.005	LysNH(ϵ)	0.080
NH7	0.005	NH2	0.173
^{2}AlaNH	0.018	NH6	>0.2
^{1}AlaNH	0.026		

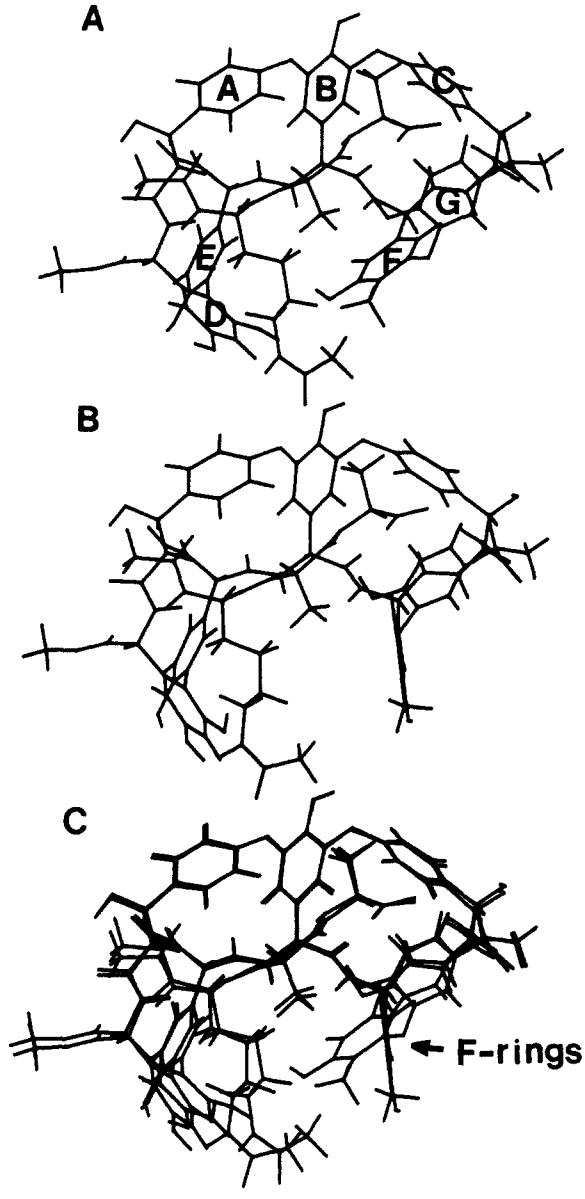

Figure 4. Structures I (A) and II (B) obtained after an energy minimization with VFF of two structures selected from the dynamics trajectory. The arrow points to the different F-ring conformations in the superimposed structures (C).

These two structures are almost equal in energy, and transitions between these two ring conformations occured several times in the short dynamics run. As shown in Table II, most of the experimentally determined distances are in good agreement with the interproton distances for either structure I or II. However, for the F-ring protons, the experimentally determined distances (F2-3′, F2-G6, F6-3′, NH4-F2) agree better with a structure somewhere between I and II. Yet, no low-energy conformation was found that supported these distances constraints. Thus, the NOE data suggest that the two F-ring conformations of the bound antibiotic as shown in structures I and II may both be present. It is interesting to note that large-scale oscillations of the F and G ring have been observed for free ristocetin, but for NMR studies in Me_2SO Williams et al.[11] reported that the conformation for this part of the ristocetin molecule becomes locked upon binding to the peptide. In contrast, the results described here suggest that the F and G ring of the antibiotic still have considerable mobility even when bound to the tripeptide.

The experimentally determined distances were also compared with the effective distances (Table II) obtained from the molecular dynamics run. Although the average distances obtained from the dynamics trajectory were closer to those obtained experimentally, especially for distances involving the F ring (F6-3′ and NH4-F2), the overall improvement was small. The fact that an exact agreement between the distances derived from the NOE data and dynamics average was not observed is not surprising. Even if other errors in the trajectory are negligible, the NOE derived distances represent an average over the NMR time scale; whereas, the dynamics run was performed for only 10 ps.

In Table III the dihedral angles calculated from the vicinal spin–spin coupling constants ($^3J_{NH-\alpha CH}$) are shown to be very similar to those measured from the energy minimized structures I and II and the average dihedral angles obtained from the structures in the dynamics calculations. Although the dihedral angles obtained experimentally agree with the computer-generated structures, the measured dihedral angles are not sensitive to subtle or even large variations in structure. For example, the NH3-3′ dihedral angle which is located next to the F ring is only 10° different in structures I and II. Yet, there is a big difference in F-ring conformations for these two structures. This demonstrates that coupling constant data are by no means sufficient to determine the structure of the complex but may provide additional supportive evidence.

Other NMR parameters that have been used in structural studies are NH temperature coefficients[27] and NH exchange rates.[28] These parameters are usually interpreted in terms of possible hydrogen bonds and solvent accesibility. Table IV lists the NH exchange rates for the amide protons of the antibiotic–peptide complex. The exchange rates of the NH protons of the bound antibiotic and tripeptide were found to be slower than the free molecules. Furthermore, those NH protons located on the inside of the complex which are postulated to be involved in hydrogen bonds (NH3, NH4) exchanged more slowly than those on the outside of the complex (NH6). The NH2 protons was an exception to this general rule. The exchange rate of the NH2 proton was found to be two orders of magnitude faster than the NH3 and NH4 protons. Yet from our NOE data (Table II), the NH2, NH3, and NH4 protons must be located on the same side of the antibiotic in a location favorable for an interaction with the carboxylate group of the tripeptide. However, predictions of hydrogen bonds based solely on NH exchange rates, especially when the effects of pH are not considered, must be treated with caution.

Conclusions

From NOEs, vicinal coupling constants, and NH exchange rates, the structure(s) of the ristocetin pseudo-aglycon-Ac_2-Lys-D-Ala-D-Ala complex has been examined. Qualitatively, the NMR data suggest that the ^{1}Ala residue is situated between the B and G aromatic rings of the antibiotic. The tripeptide extends toward the C terminus of the antibiotic with the middle ^{2}Ala residue located near the E ring. For the Lys residue, our NOE data suggest that the α-$COCH_3$ protons are close to the A6, A_{Bz}, and ristosamine sugar attached to residue 6 with the Lys side chain extending over the D ring of the antibiotic. The location of the two D-Ala residues is in agreement with previous structural studies of ristocetin–peptide complexes. However, our results on the location of the Lys side chain are different from previous NMR studies. Williams and co-workers[11] postulated that, although less precisely defined, the lysine side chain is located in the direction of the A ring in both vancomycin and ristocetin–tripeptide complexes in Me_2SO solution. Our results are consistent with a model

(27) Kalman, J. R.; Williams, D. H. *J. Am. Chem. Soc.* **1980**, *102*, 906.
(28) Woodward, C. K.; Hilton, B. D. *Annu. Rev. Biophys. Bioeng.* **1979**, *8*, 99.

proposed[12] for the β-avoparcin-Ac_2-Lys-D-Ala-D-Ala complex and a more recent report[13] on the structure of the ristocetin-tripeptide complex in aqueous solution in which the lysine side chain is over the D ring of the antibiotic.

From a quantitative analysis of our NOE data, it was concluded that no one structure could fit all of the NMR data. By including an additional pseudobond term in the force field used to model the complex, we were able to produce a structure which agreed with the observed proton-proton distances included as constraints. Relaxing the pseudobond constraint, however, produced a structure with several distances not in accord with observations. Through the use of molecular dynamics calculations, additional structures were generated which compared more favorably to the NOE derived distances. By obtaining many proton-proton distances as accurately as possible and employing molecular dynamics calculations, dynamic averaging effects were considered in the interpretation of the measured NMR parameters. These methods allowed us to obtain detailed structural information which may prove to be important in the rational design of pharmaceutical agents. The general methodology described here is currently being refined and applied in structural studies of other physiologically important molecules.[29]

Acknowledgment. The authors thank E. R. P. Zuiderweg for writing the 2D base line correction routine used in the data processing and G. Bolis for modifying the VFF program to include the NOE derived distance constraints.

(29) Fesik, S. W.; Holleman, W. H.; Perun, T. J. *Biochem. Biophys. Res. Commun.* **1985**, *131*, 517.
(30) Tropp, J. *J. Chem. Phys.* **1980**, *72*, 6035.
(31) Bystrov, V. F. In *Progress in NMR Spectroscopy*; Pergamon Press: Great Britain, 1976; Vol. 10, pp 41-81.

Optical Detection of Paramagnetic Resonance by Magnetic Circular Dichroism. Applications to Aqueous Solutions of Metalloproteins

Christopher P. Barrett,[†] Jim Peterson,[†] Colin Greenwood,[‡] and Andrew J. Thomson*[†]

Contribution from the School of Chemical Sciences and School of Biological Sciences, University of East Anglia, Norwich NR4 7TJ, U.K. *Received September 9, 1985*

Abstract: An apparatus has been assembled to enable microwave resonance of a ground electronic state to be detected by measuring the intensity of the magnetic circular dichroism (MCD) spectrum. The sample is mounted in a rectangular *Q*-band cavity resonating in the TE_{102} mode which can be lowered into the center of a split-coil superconducting magnet. The circular dichroism signal is measured with a JASCO-J500D spectropolarimeter, a monochromatic optical beam of differentially circularly polarized light being passed along the magnetic field axis of the solenoid and through the microwave cavity. This apparatus has been used to measure the MCD-detected optical double microwave resonance (ODMR) of frozen aqueous solutions of Cu^{II}(EDTA) and copper(II) azurin, a blue copper protein obtained from *Pseudomonas aeruginosa*. The line shapes of the MCD-ODMR spectrum are the same as in the *Q*-band EPR spectrum only in the case that the optical transition is isotropic, as appears to be the case for Cu^{II}(EDTA). The MCD-ODMR spectrum of azurin has been measured at four optical wavelengths, 460, 640, 750, and 1000 nm, corresponding to the positions of the major features in the MCD spectrum. These bands arise from charge-transfer transitions from cysteine and histidine ligand-to-copper(II) $d_{x^2-y^2}$ orbitals. The MCD-ODMR detects only the *z* component of the ground-state *g* tensor. A simple computer simulation shows that this implies that the MCD transitions at these wavelengths arise from *x,y*-polarized bands. The shapes of the MCD-ODMR lines hence provide a method of determining the polarizations of optical transitions relative to one another and to the ground-state *g*-tensor axes of a paramagnetic species in frozen solutions. The MCD spectrum can be partially quenched by application of microwave power when the microwave photon energy is equal to the ground-state Zeeman energy. In this way it is possible to deconvolute the MCD spectrum of a chromophore even though several different species are present with overlapping optical spectra. This appears to be the first application of the technique of MCD-ODMR to frozen aqueous solutions and to the study of metalloproteins. The technique promises to yield much useful information about the electronic and molecular structure of transition-metal ions in proteins.

Low-temperature magnetic circular dichroism (MCD) spectroscopy is now well established as a useful optical probe of the ground-state magnetic properties of metal centers in metalloproteins.[1-3] Using suitable mixtures of glassing agents, aqueous solutions of protein can be cooled to liquid helium temperatures, yielding samples of sufficiently good optical quality to enable reliable MCD spectra to be measured. Paramagnetic metal centers give temperature- and magnetic field-dependent MCD signals in the region of their optical absorption bands. The temperature dependence is a consequence of the Boltzmann population distribution among the Zeeman-split sublevels which results in the differential absorption of left-minus-right circularly polarized light.[4] A plot of the intensity of the MCD signal at a fixed wavelength against B/T, where B is the magnetic field and T the absolute temperature, constitutes a magnetization curve. Analysis of the form of the curve in favorable cases enables the ground-state *g* values and spin S to be determined.[1] An optical probe of

[†]School of Chemical Sciences.
[‡]School of Biological Sciences.

(1) Thomson, A. J.; Johnson, M. K. *Biochem. J.* **1980**, *191*, 411.
(2) For a recent review of results on metalloproteins, excluding heme, see: (a) Johnson, M. K.; Robinson, A. E.; Thomson, A. J. In *Iron Sulfur Proteins*; Spiro, T. G., *Ed.*; Wiley: New York 1982; Vol. 4, Chapter 10. (b) Dooley, D. M.; Dawson, J. H. *Coord. Chem. Rev.* **1984**, *60*, 1.
(3) For examples of applications to heme-containing systems, see: (a) Walsh, T. A.; Johnson, M. K.; Greenwood, C.; Barber, D.; Springall, J. P. *Biochem. J.* **1979**, *177*, 29. (b) Thomson, A. J.; Johnson, M. K., Greenwood, C.; Gooding, P. E. *Biochem. J.* **1981**, *193*, 687. (c) Brittain, T.; Greenwood, C.; Springall, J. P.; Thomson, A. J. *Biochim. Biophys. Acta* **1982**, *703*, 117. (d) Thomson, A. J.; Eglinton, D. G.; Hill, B. C.; Greenwood, C. *Biochem. J.* **1982**, *207*, 167.
(4) Stephens, P. J. *Adv. Chem. Phys.* **1976**, *35*, 197.

0002-7863/86/1508-3170$01.50/0